

Article

Force Analysis of Masonry Cave-Dwelling Structure Based on Elastic Center Method

Yan'e Hao ^{1,*}  and Yongqiang Lan ²¹ College of Architecture and Engineering, Yan'an University, Yan'an 716000, China² Department of Basic Construction, Yan'an University, Yan'an 716000, China

* Correspondence: hyeyau2021@yau.edu.cn; Tel.: +86-153-1958-6499

Abstract: The cave dwelling is one of the most typical traditional dwellings and green building forms in the Loess Plateau of Northern Shaanxi. The construction of the cave dwelling was built only based on the experience passed down by predecessors, without the guidance of formal design theories and calculation methods, and the overall safety of the cave-dwelling structure needs to be solved urgently. To make the mechanical analysis model closer to the actual force of the masonry cave dwelling, it is proposed to simplify the arch ring in the masonry cave-dwelling structure into an unhinged arch mechanical calculation model. Applying the theory of elastic center to the force method calculation in structural mechanics, the force of the cave-dwelling structure is analyzed and compared with the force results of the three-hinged arch calculation model, so as to determine the correctness and reliability of the calculation diagram of the unhinged arch. The conclusions indicate it is correct and reliable to use the unhinged arch calculation model, which is closer to the actual force situation, to calculate the forces of the arch rings in masonry cave dwellings, and both the three-hinged arch and unhinged arch models are feasible to be applied to the mechanical analysis of the arch rings. The unhinged arch calculation model is more reliable and safer in the design and calculation of the cave-dwelling leg components compared with the three-hinged arch calculation model because it considers the bending moment at the arch foot support. The research results can be used to improve the structural design data of the cave dwelling and provide theoretical guidance for the construction, repair, and protection of the cave dwelling.



Citation: Hao, Y.; Lan, Y. Force Analysis of Masonry Cave-Dwelling Structure Based on Elastic Center Method. *Appl. Sci.* **2023**, *13*, 4292. <https://doi.org/10.3390/app13074292>

Academic Editor: Giuseppe Lacidogna

Received: 28 February 2023

Revised: 23 March 2023

Accepted: 24 March 2023

Published: 28 March 2023



Copyright: © 2023 by the authors. Licensee MDPI, Basel, Switzerland. This article is an open access article distributed under the terms and conditions of the Creative Commons Attribution (CC BY) license (<https://creativecommons.org/licenses/by/4.0/>).

Keywords: elastic center; force method; cave dwelling; force analysis

1. Introduction

Cave dwellings are widely distributed in the Loess Plateau of Northwest China. They are one of the most typical traditional dwellings in northern Shaanxi. In addition, they are favored by local residents for their advantages of adapting to the climate, using local materials, having a low cost, being warm in winter and cool in summer, and, particularly, the covering soil on the upper part of the cave dwelling being able to make use of its own temperature and heat insulation function. They are also known as energy-saving ecological residences. According to the different ways of construction, cave dwellings can be divided into three categories [1]: One is the excavation pattern cave dwelling, which includes the cliff-side-type loess cave dwelling excavated directly from the loess cliff face; the patio-type loess cave dwelling which was excavated along the four walls in the manually excavated square earth pit; and the earth-pit-type cave-dwelling which was excavated in a naturally formed earth pit, as shown in Figure 1a,b [1]. The second is the masonry pattern cave dwelling; that is, the free-standing cave dwelling or open hoop cave dwelling is an earth cave dwelling, brick cave dwelling, or stone cave dwelling directly hoop-built on the flat ground, and the upper part is covered with a certain thickness of soil, as shown in Figure 1c. The third is the half excavation and half masonry pattern cave dwelling, that is, the interface cave dwelling; a section of the masonry arch ring is connected to the mouth of the loess

cave dwelling to prevent the cliff surface from collapsing, as shown in Figure 1d. With the improvement of people's living conditions and the convenience of production and living conditions, masonry cave dwellings have sprung up. However, the construction of masonry cave dwellings is based on experience without structural calculation and stress analysis, and the construction method lacks theoretical guidance, which causes the hidden dangers of the cave structures to occur from time to time. Cave-dwelling buildings are the concentrated carrier of the local residents' construction skills, survival wisdom, geographical environment, regional culture, and social economy, and they are a valuable architectural and cultural heritage. The in-depth studies on their stress have an important scientific significance and social value for the protection and inheritance of these traditional local-style dwellings.

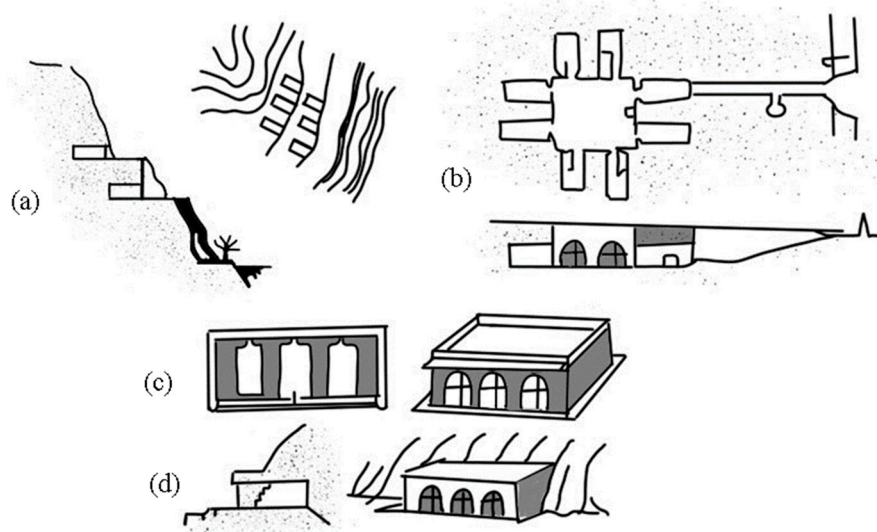


Figure 1. Three categories of cave dwellings: (a) and (b) excavation pattern; (c) masonry pattern; and (d) half excavation and half masonry pattern.

The cave dwellings are classified as earth-sheltered architectures that have been much studied by foreign scholars [2–6]. To preserve this valuable architectural heritage, Chinese scholars have carried out a great deal of research on it. In recent years, many scholars have focused on the structural principle [7,8], stress characteristics [9–11], stability analysis under different influencing factors [12–19], the effect of water on the stability of the cave dwelling [20,21], and the reinforcement and protection measures using new materials and advanced methods for the loess cliff-side cave dwelling and earth-pit-type cave dwelling [22–26]. However, there is little research on the masonry cave dwelling. F.J. Wang et al. [27] combined the actual earthquake damage with numerical simulation experiments; the vertical displacement of the arch vault and the ratio of the vault height to the calculated span were proposed as the damage indicators for the free-standing cave dwelling under an earthquake. Y.M. Yan et al. [28,29] carried out a stress analysis and cross-sectional calculations on the arch ring of a stone masonry cave dwelling which adopted the three-hinged arch calculation model, but the arch axis was chosen as a reasonable arch axis (catenary), which did not match the curved arch axis in the actual cave dwelling. Y.X. Zhang et al. [30] analyzed the common failure forms of the cave dwellings and the stress of the most common semi-open and semi-dark cave dwellings built with adobe, and used the “equal-substituted three-hinged arch” method to calculate only the reaction forces of the vault and the foot of the arch, without an internal force analysis of any section of the arch ring. C.H. Huang et al. [31] divided the cave-dwelling structure into the dome parts and column parts. The calculation model of the dome structure was a two-hinged semi-circular arch. The internal force coefficient of the arch was determined by consulting the manual of the static force calculation, and the internal forces of the arch vault and arch foot of

the semi-circular arch shaft cave dwelling were calculated. However, the unified internal force calculation formula of the circular arch cave dwelling was not deduced. Therefore, the applicability of this calculation method is not strong. In the above works of literature, the arch feet of the cave dwelling were simplified as a fixed hinge support; the bending moment of the arch ring at the arch feet was not considered.

In order to make the mechanical analysis model closer to the actual force situation of the masonry cave dwelling, the calculation model of an unhinged arch is proposed here for the arch ring part of the masonry cave-dwelling structure. Based on the elastic center method [32,33], the unified internal force calculation formula of the circular arc arch ring in the masonry cave-dwelling structure is deduced by using the principle of force method; at the same time, it is compared with the stress calculation results of the three-hinged arch to clarify the influence of considering the arch ring support of the cave dwelling as a fixed hinged support. This has a certain theoretical reference value for the construction, reinforcement, and protection of the masonry cave dwelling, and further supplements and improves the design data of cave-dwelling building structures.

2. Research Object and Methodology

The basic construction of the masonry cave dwelling is shown in Figure 2. The actual picture is shown in Figure 3. This structure can be regarded as being composed of the upper arch ring and the lower cave-dwelling legs. The arch ring is a bending member and the cave-dwelling legs are compression members [24]. The force calculation and analysis of the masonry cave-dwelling structure can be simplified to a plane strain problem. If the arch foot support is simplified to a fixed support, the calculation model of the upper arch ring is a symmetrical fixed unhinged arch, as shown in Figure 4a. The elastic center method is equivalent to the original unhinged arch to the unhinged arch with a rigid arm, which can be seen in Figure 4b. We determine the length of the rigid arm, that is, the position of the elastic center, lead the endpoint of the rigid arm to the elastic center, and then take the basic system with the rigid arm so that all the secondary coefficients in the force method equation are equal to zero. At this time, the equation of the force method is simplified to three independent one-dimensional linear equations, which greatly reduces the computational workload.

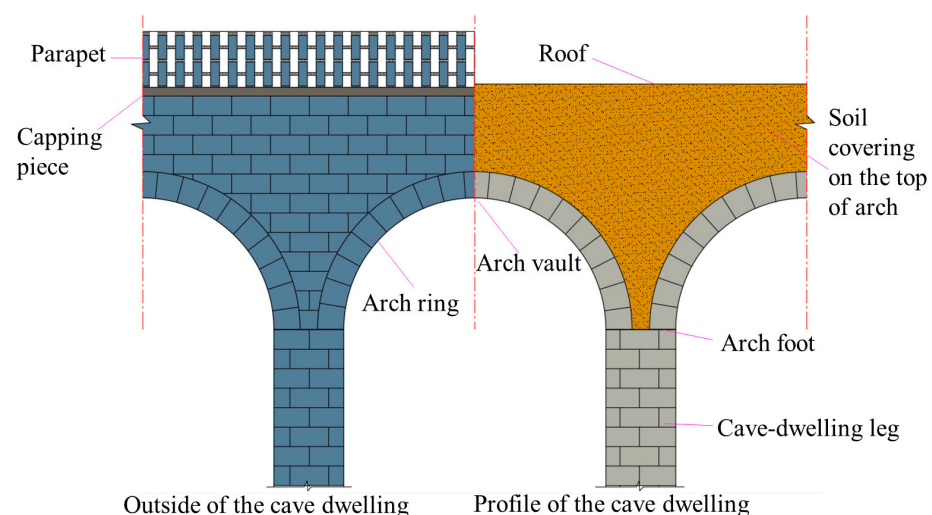


Figure 2. Construction of the masonry cave dwelling.



Figure 3. Real picture of the masonry cave dwelling.

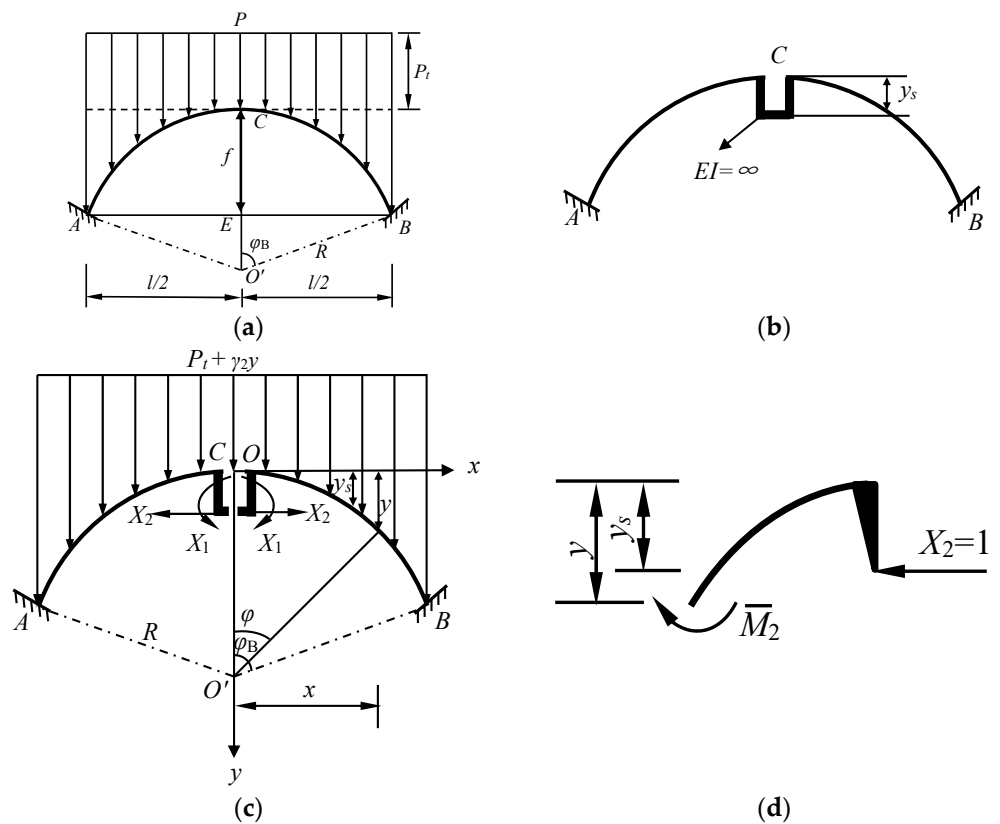


Figure 4. Unhinged arch model based on elastic center method: (a) unhinged arch calculation diagram of the arch ring; (b) equivalent unhinged arch with rigid arms; (c) basic system with rigid arm; and (d) force diagram of the isolated part.

2.1. Loads on the Masonry Cave Dwelling

It can be seen from Figures 2 and 3 that the loads on the masonry cave dwelling mainly include the self-weight of the arch ring, the self-weight of the filling, and the live loads on the head (roof). Due to the small drainage slope of the roof, the filling surface is approximately taken as a horizontal surface, and the live loads are mainly snow load, vehicle, pedestrian, or construction live load, which can be considered to be uniformly distributed. Assuming that the arch ring is of equal thickness, the self-weight of the arch ring and the self-weight of the filling vary in size with the axis of the arch ring. In order to simplify the calculation, it is assumed that the load is continuously distributed without interruption and mutation along the span length of the arch, as shown in Figure 4. Bending stiffness $EI = \text{constant}$. Then, the load concentration at any section of the arch ring is as follows:

$$P = P_t + \gamma_2 y = \gamma_1 h_1 + \gamma_2 h_2 + \gamma_2 y + \psi q \quad (1)$$

where P_t is the vertical uniformly distributed load concentration, and $P_t = \gamma_1 h_1 + \gamma_2 h_2 + \psi q$; γ_1 and γ_2 are the gravity density of the arch ring and the gravity density of the covering soil, respectively; h_1 and h_2 are the thickness of the arch ring and the thickness of the soil covering on the top of arch, respectively; y is the longitudinal co-ordinate of the arch ring axis; ψ is the combined value coefficient of the live load, taking into account the finite effect of the live load—0.7 is taken here; and q is the live load of the roof, taken as 2.0 kN/m².

2.2. Basic Assumptions Adopted in the Calculation Diagram

Considering the construction characteristics of masonry cave-dwelling structure, the following assumptions are adopted when determining the calculation diagram:

- Because the curve form of the arch axis has little effect on the internal force results, the upper arch ring of the cave dwelling is simplified as a circular arc axis with equal sections;
- The support constraint between the arch foot and the lower cave-dwelling leg is assumed to be fixed; that is, the arch foot is considered to resist bending;
- Generally, the ratio of the arch height f to the arch span length l is greater than 0.2, so when calculating the coefficients and free terms of the force method equation, only the influence of bending deformation is considered, and the effect of shear force and axial force on deformation is ignored.

2.3. Derivation of Internal Force Calculation Formula Based on Unhinged Arch Model

The selected basic system of force method based on unhinged arch model is shown in Figure 4c. Applying the elastic center theory, the internal force calculation formula of an unhinged arch can be quickly deduced.

2.3.1. Equation of Arc Arch-Axis

As shown in Figure 4a, the cave-dwelling span is l and the arch ring height is f ; then, the radius R of the arc arch ring shall be:

$$R^2 = \left(\frac{l}{2}\right)^2 + (R - f)^2 \quad (2)$$

so

$$R = \frac{l^2 + 4f^2}{8f} \quad (3)$$

The central angle φ_B of the half arch is:

$$\sin \varphi_B = \frac{l/2}{R}, \cos \varphi_B = \frac{R - f}{R} \quad (4)$$

As shown in Figure 4c, the co-ordinate origin O is located at the vault of arc (C), to the right as the x -axis and down as the y -axis; the equation of the axis of the arch ring can also be written as:

$$x = R \sin \varphi, y = R - R \cos \varphi \tag{5}$$

2.3.2. Position of the Elastic Center

As shown in Figure 4c, the elastic center y_s is:

$$y_s = \int \frac{y}{EI} ds / \int \frac{1}{EI} ds = \frac{2}{EI} \int_0^{\varphi_B} R(1 - \cos \varphi) R d\varphi / \frac{2}{EI} \int_0^{\varphi_B} R d\varphi = \frac{\varphi_B - \sin \varphi_B}{\varphi_B} R \tag{6}$$

2.3.3. Internal Force of Basic Structure under Unit Force

When the basic structure is under the action of $X_1 = 1$, the internal forces are calculated as follows:

$$\overline{M}_1 = 1, \overline{Q}_1 = 0, \overline{N}_1 = 0 \tag{7}$$

When the basic structure is under the action of $X_2 = 1$, according to the equilibrium condition of the isolated part in Figure 4d, the following equation of bending moment is established:

$$\begin{aligned} \overline{M}_2 &= y - y_s = R(1 - \cos \varphi) - \left(\frac{\varphi_B - \sin \varphi_B}{\varphi_B} \right) R \\ &= R \left(\frac{\sin \varphi_B}{\varphi_B} - \cos \varphi \right) \end{aligned} \tag{8}$$

Shear force and axial force are, respectively:

$$\overline{Q}_2 = \sin \varphi, \overline{N}_2 = -\cos \varphi \tag{9}$$

2.3.4. Bending Moment of Basic Structure under Load

Under the load P , the bending moment equation of any section of the cantilever curved beam is:

$$M_P(x) = -\frac{P_t}{2} x^2 - \left(x \int_0^x \gamma_2 y dx - \int_0^x x \gamma_2 y dx \right) \tag{10}$$

Substituting (5) into (10), we obtain:

$$\begin{aligned} M_P(\varphi) &= -\frac{P_t}{2} R^2 \sin^2 \varphi - \gamma_2 R \sin \varphi \int_0^\varphi (R - R \cos \varphi) d(R \sin \varphi) \\ &\quad + \gamma_2 \int_0^\varphi R \sin \varphi (R - R \cos \varphi) d(R \sin \varphi) \\ &= -\frac{P_t}{2} R^2 \sin^2 \varphi - \gamma_2 R^3 \sin \varphi \int_0^\varphi (\cos \varphi - \cos^2 \varphi) d\varphi \\ &\quad + \gamma_2 R^3 \int_0^\varphi (\sin \varphi \cos \varphi - \sin \varphi \cos^2 \varphi) d\varphi \\ &= -\frac{P_t}{2} R^2 \sin^2 \varphi - \gamma_2 R^3 \sin \varphi \left[\sin \varphi - \left(\frac{\varphi}{2} + \frac{\sin 2\varphi}{4} \right) \right]_0^\varphi \\ &\quad + \gamma_2 R^3 \left[\frac{\sin^2 \varphi}{2} + \frac{\cos^3 \varphi}{3} \right]_0^\varphi \\ &= -\frac{P_t}{2} R^2 \sin^2 \varphi - \gamma_2 R^3 \left(\frac{\sin^2 \varphi}{2} - \frac{\varphi \sin \varphi}{2} - \frac{\sin \varphi \sin 2\varphi}{4} - \frac{\cos^3 \varphi}{3} + \frac{1}{3} \right) \end{aligned} \tag{11}$$

2.3.5. Calculation of Principal Coefficients and Free Items

After substituting (6)–(8) and (11), we get:

$$EI \delta_{11} = \int \overline{M}_1^2 ds = 2 \int_0^{\varphi_B} R d\varphi = 2R\varphi_B = a_1 R \tag{12}$$

where:

$$a_1 = 2R \tag{13}$$

$$\begin{aligned}
 EI\delta_{22} &= \int \overline{M}_2^2 ds = 2 \int_0^{\varphi_B} \left[R \left(\frac{\sin \varphi_B}{\varphi_B} - \cos \varphi \right) \right]^2 R d\varphi \\
 &= 2R^3 \int_0^{\varphi_B} \left(\frac{\sin^2 \varphi_B}{\varphi_B^2} - 2 \cos \varphi \frac{\sin \varphi_B}{\varphi_B} + \cos^2 \varphi \right) d\varphi \\
 &= 2R^3 \left[\frac{\sin^2 \varphi_B}{\varphi_B^2} \varphi - 2 \sin \varphi \frac{\sin \varphi_B}{\varphi_B} + \left(\frac{\varphi}{2} + \frac{\sin 2\varphi}{4} \right) \right]_0^{\varphi_B} \\
 &= R^3 \left(-\frac{2 \sin^2 \varphi_B}{\varphi_B} + \frac{\sin 2\varphi_B}{2} + \varphi_B \right) \\
 &= a_2 R^3
 \end{aligned}
 \tag{14}$$

where:

$$a_2 = \left(-\frac{2 \sin^2 \varphi_B}{\varphi_B} + \frac{\sin 2\varphi_B}{2} + \varphi_B \right)
 \tag{15}$$

Free items are:

$$\begin{aligned}
 EI\Delta_{1P} &= \int \overline{M}_1 M_P(\varphi) ds \\
 &= -2\gamma_2 R^3 \int_0^{\varphi_B} 1 \times \left(\frac{\sin^2 \varphi}{2} - \frac{\varphi \sin \varphi}{2} - \frac{\sin \varphi \sin 2\varphi}{4} - \frac{\cos^3 \varphi}{3} + \frac{1}{3} \right) R d\varphi \\
 &\quad + 2 \int_0^{\varphi_B} 1 \times \left(-\frac{P_t}{2} R^2 \sin^2 \varphi \right) R d\varphi \\
 &= -\gamma_2 R^4 \left[\left(\frac{\varphi}{2} - \frac{\sin 2\varphi}{4} \right) + (\varphi \cos \varphi - \sin \varphi) - \frac{\sin^3 \varphi}{3} - \frac{2}{3} \left(\sin \varphi - \frac{\sin^3 \varphi}{3} \right) + \frac{2}{3} \varphi \right]_0^{\varphi_B} \\
 &\quad - P_t R^3 \left[\frac{\varphi}{2} - \frac{\sin 2\varphi}{4} \right]_0^{\varphi_B} \\
 &= -\gamma_2 R^4 \left(\frac{7\varphi_B}{6} - \frac{\sin 2\varphi_B}{4} + \varphi_B \cos \varphi_B - \frac{5 \sin \varphi_B}{3} - \frac{\sin^3 \varphi_B}{9} \right) \\
 &\quad - P_t R^3 \left(\frac{\varphi_B}{2} - \frac{\sin 2\varphi_B}{4} \right) \\
 &= -b_2 R^4 - b_1 P_t R^3
 \end{aligned}
 \tag{16}$$

where:

$$b_1 = \frac{\varphi_B}{2} - \frac{\sin 2\varphi_B}{4}, b_2 = \gamma_2 \left(\frac{7\varphi_B}{6} - \frac{\sin 2\varphi_B}{4} + \varphi_B \cos \varphi_B - \frac{5 \sin \varphi_B}{3} - \frac{\sin^3 \varphi_B}{9} \right)
 \tag{17}$$

$$\begin{aligned}
 EI\Delta_{2P} &= \int \overline{M}_2 M_P(x) ds = \int (y - y_s) M_P(x) ds = \int R \left(\frac{\sin \varphi_B}{\varphi_B} - \cos \varphi \right) M_P(\varphi) ds \\
 &= -2\gamma_2 R^4 \int_0^{\varphi_B} \left(\frac{\sin \varphi_B}{\varphi_B} - \cos \varphi \right) \times \left(\frac{\sin^2 \varphi}{2} - \frac{\varphi \sin \varphi}{2} - \frac{\sin \varphi \sin 2\varphi}{4} - \frac{\cos^3 \varphi}{3} + \frac{1}{3} \right) R d\varphi \\
 &\quad + 2R \int_0^{\varphi_B} \left(\frac{\sin \varphi_B}{\varphi_B} - \cos \varphi \right) \times \left(-\frac{P_t}{2} R^2 \sin^2 \varphi \right) R d\varphi \\
 &= -\gamma_2 R^5 \frac{\sin \varphi_B}{\varphi_B} \int_0^{\varphi_B} \left(\sin^2 \varphi - \varphi \sin \varphi - \frac{\sin \varphi \sin 2\varphi}{2} - \frac{2 \cos^3 \varphi}{3} + \frac{2}{3} \right) d\varphi \\
 &\quad + \gamma_2 R^5 \int_0^{\varphi_B} \left(\sin^2 \varphi \cos \varphi - \varphi \sin \varphi \cos \varphi - \frac{\sin^2 2\varphi}{4} - \frac{2 \cos^4 \varphi}{3} + \frac{2 \cos \varphi}{3} \right) d\varphi \\
 &\quad - P_t R^4 \int_0^{\varphi_B} \left(\frac{\sin \varphi_B}{\varphi_B} \sin^2 \varphi - \sin^2 \varphi \cos \varphi \right) d\varphi \\
 &= -\gamma_2 R^5 \frac{\sin \varphi_B}{\varphi_B} \left(\frac{7\varphi_B}{6} - \frac{\sin 2\varphi_B}{4} + \varphi_B \cos \varphi_B - \frac{5 \sin \varphi_B}{3} - \frac{\sin^3 \varphi_B}{9} \right) \\
 &\quad + \gamma_2 R^5 \left(\frac{\sin^3 \varphi_B}{3} - \frac{7 \sin 2\varphi_B}{24} + \frac{\varphi_B \cos 2\varphi_B}{4} - \frac{3\varphi_B}{8} + \frac{\sin 4\varphi_B}{96} + \frac{2 \sin \varphi_B}{3} \right) \\
 &\quad - P_t R^4 \left(\frac{\sin \varphi_B}{2} - \frac{\sin 2\varphi_B \sin \varphi_B}{4\varphi_B} - \frac{\sin^3 \varphi_B}{3} \right) \\
 &= -(b_4 - b_5) R^5 - b_3 P_t R^4
 \end{aligned}
 \tag{18}$$

where:

$$b_3 = \left(\frac{\sin \varphi_B}{2} - \frac{\sin 2\varphi_B \sin \varphi_B}{4\varphi_B} - \frac{\sin^3 \varphi_B}{3} \right)
 \tag{19}$$

$$b_4 = \gamma_2 \frac{\sin \varphi_B}{\varphi_B} \left(\frac{7\varphi_B}{6} - \frac{\sin 2\varphi_B}{4} + \varphi_B \cos \varphi_B - \frac{5 \sin \varphi_B}{3} - \frac{\sin^3 \varphi_B}{9} \right) \quad (20)$$

$$b_5 = \gamma_2 \left(\frac{\sin^3 \varphi_B}{3} - \frac{7 \sin 2\varphi_B}{24} + \frac{\varphi_B \cos 2\varphi_B}{4} - \frac{3\varphi_B}{8} + \frac{\sin 4\varphi_B}{96} + \frac{2 \sin \varphi_B}{3} \right) \quad (21)$$

2.3.6. Solving the Force Method Equation

The force method equation of this structure is:

$$\left. \begin{aligned} \delta_{11}X_1 + \Delta_{1P} &= 0 \\ \delta_{22}X_2 + \Delta_{2P} &= 0 \end{aligned} \right\} \quad (22)$$

Substitute Formulae (12), (14), (16) and (18) into Equation (22) to get:

$$\left. \begin{aligned} a_1RX_1 - P_t b_1 R^3 - b_2 R^4 &= 0 \\ a_2 R^3 X_2 - P_t b_3 R^4 - (b_4 - b_5) R^5 &= 0 \end{aligned} \right\} \quad (23)$$

From the above Equation (23), the redundant unknown forces X_1 and X_2 are obtained:

$$X_1 = -\frac{\Delta_{1P}}{\delta_{11}} = \frac{P_t b_1 R^2 + b_2 R^3}{a_1}, X_2 = -\frac{\Delta_{2P}}{\delta_{22}} = \frac{P_t b_3 R + (b_4 - b_5) R^2}{a_2} \quad (24)$$

By substituting Formulae (13), (15), (17) and (19)–(21) into Formula (24), the specific values of the redundant unknown forces X_1 and X_2 can be obtained.

2.3.7. Calculation of the Internal Force of the Vault and the Foot of Arch

For the vault of the arch, it can be calculated as follows:

Bending moment:

$$M_C = X_1 - X_2 \cdot y_s \quad (25)$$

Axial force:

$$N_C = X_2 \quad (26)$$

The force diagram for the right half-arch ring is shown in Figure 5.

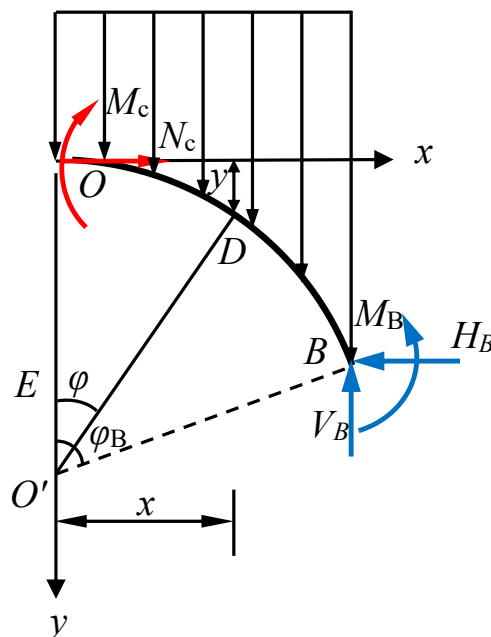


Figure 5. Force diagram of the right half-arch ring.

For the foot of the arch, it can be calculated as follows:
 Bending moment:

$$M_B = \bar{M}_1 X_1 + \bar{M}_2 X_2 + M_P$$

$$= X_1 + (f - y_s) X_2 - \frac{P_t}{2} x_B^2 - \gamma_2 R^3 \left(\frac{\sin^2 \varphi_B}{2} - \frac{\varphi_B \sin \varphi_B}{2} - \frac{\sin \varphi_B \sin 2\varphi_B}{4} - \frac{\cos^3 \varphi_B}{3} + \frac{1}{3} \right) \quad (27)$$

Horizontal thrust:

$$H_B = N_C = X_2 \quad (28)$$

The vertical reaction force V_B of the arch foot is a total load of half span, which is:

$$V_B = \int_0^{\frac{l}{2}} P dx = \frac{P_t l}{2} + \int_0^{\frac{l}{2}} \gamma_2 y dx = \frac{P_t l}{2} + \gamma_2 R^2 \left(\sin \varphi_B - \frac{\varphi_B}{2} - \frac{\sin 2\varphi_B}{4} \right) \quad (29)$$

2.3.8. Internal Force Calculation Formula of Any Section of the Arch Ring

The force diagram of any section of the right half-arch ring is shown in Figure 6. According to the equilibrium conditions, the internal force calculation formula of any section of the right half-arch ring are as follows:

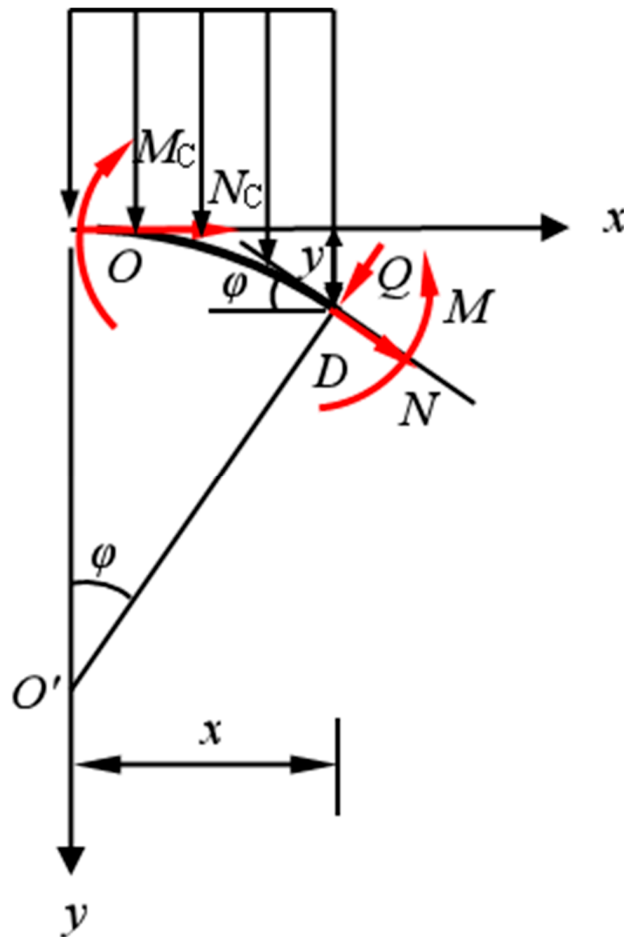


Figure 6. Force diagram of any section of the right half-arch ring.

Bending function equation:

$$M(\varphi) = \bar{M}_1 X_1 + \bar{M}_2 X_2 + M_P$$

$$= X_1 + X_2 R \left(\frac{\sin \varphi_B}{\varphi_B} - \cos \varphi \right) - \frac{P_t}{2} R^2 \sin^2 \varphi$$

$$- \gamma_2 R^3 \left(\frac{\sin^2 \varphi}{2} - \frac{\varphi \sin \varphi}{2} - \frac{\sin \varphi \sin 2\varphi}{4} - \frac{\cos^3 \varphi}{3} + \frac{1}{3} \right) \quad (30)$$

Shear force function equation:

$$\begin{aligned}
 Q(\varphi) &= N_C \sin \varphi - \left(\int_0^x P dx\right) \cos \varphi \\
 &= X_2 \sin \varphi - P_t R \sin \varphi \cos \varphi - \left[\gamma_2 \int_0^\varphi (R - R \cos \varphi) d(R \sin \varphi)\right] \cos \varphi \quad (31) \\
 &= X_2 \sin \varphi - P_t R \sin \varphi \cos \varphi - \gamma_2 R^2 \cos \varphi \left(\sin \varphi - \frac{\varphi}{2} - \frac{\sin 2\varphi}{4}\right)
 \end{aligned}$$

Axial force function equation:

$$\begin{aligned}
 N(\varphi) &= -N_C \cos \varphi - \left(\int_0^x P dx\right) \sin \varphi \\
 &= -X_2 \cos \varphi - P_t R \sin^2 \varphi - \left[\gamma_2 \int_0^\varphi (R - R \cos \varphi) d(R \sin \varphi)\right] \sin \varphi \quad (32) \\
 &= -X_2 \cos \varphi - P_t R \sin^2 \varphi - \gamma_2 R^2 \sin \varphi \left(\sin \varphi - \frac{\varphi}{2} - \frac{\sin 2\varphi}{4}\right)
 \end{aligned}$$

The bending moment and axial force of any section of the left half-arch ring are symmetrically equal to those of the right half-arch ring, while the shear force is equal in magnitude and opposite in direction.

2.4. Internal Force Calculation Formula of Three-Hinged Arch Model

2.4.1. Three-Hinged Arch Calculation Model

In the previous calculation model of the three-hinged arch, the bending moments of the arch ring at the arch feet in the masonry cave dwelling were often ignored, and the arch feet were directly simplified as a fixed hinge support. We consider the closing effect of the left and right arch rings at the vault during masonry, and the vault was simplified as a hinge node; that is, the bending moment at the vault of the arch was regarded as zero. The stress model is shown in Figure 7.

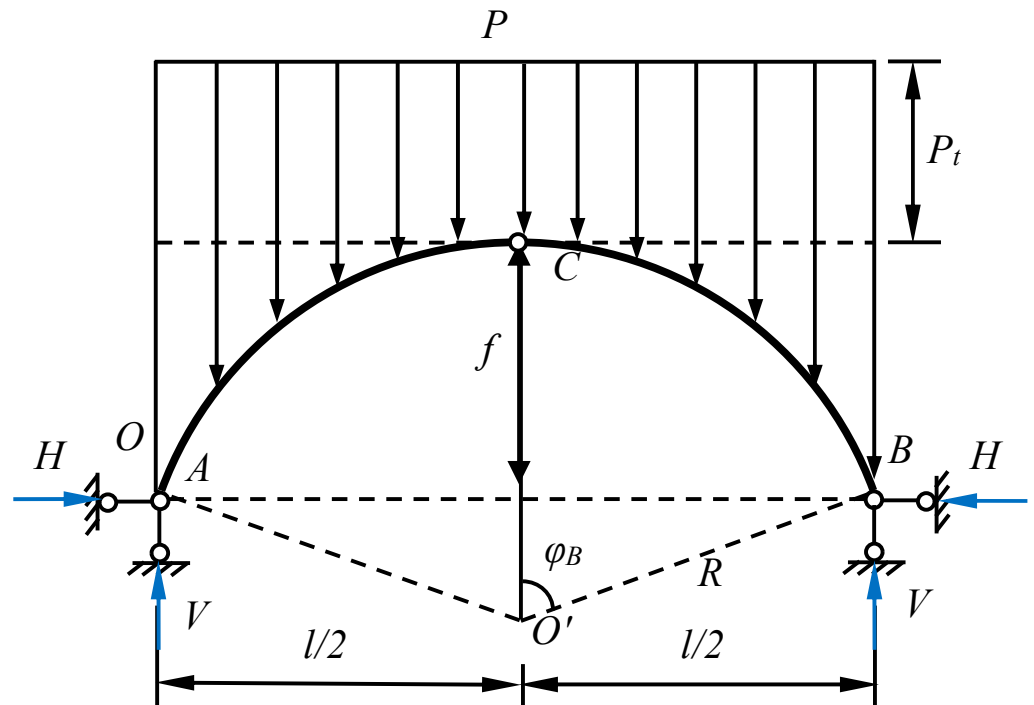


Figure 7. Three-hinged arch calculation model of arch ring.

2.4.2. Co-Ordinate Axis Setting and Arch-Axis Equation

The co-ordinate origin O is also set in the vault C, to the right for the x-axis, and down for the y-axis. The arch-axis equation is the same as Formula (5).

2.4.3. Simplification of Calculation Model and Calculation of Support Reaction Force

Because of the symmetrical structure and load, the shear force of the vault is $Q_C = 0$. The three-hinged arch calculation model can be simplified to a half-side structure and its force diagram is shown in Figure 8. Under the action of the load P of the structure, the horizontal reaction force H of the support is:

$$\begin{aligned}
 H &= \frac{1}{f} \int_0^{\frac{l}{2}} \left(\frac{l}{2} - x\right) (P_t + \gamma_2 y) dx \\
 &= \frac{1}{f} \left[\frac{P_t l^2}{8} + \frac{1}{2} \gamma_2 R^2 \left(\sin \varphi_B - \frac{\varphi_B}{2} - \frac{\sin 2\varphi_B}{4} \right) - \gamma_2 R^3 \left(\frac{\sin^2 \varphi_B}{2} + \frac{\cos^3 \varphi_B}{3} - \frac{1}{3} \right) \right] \tag{33}
 \end{aligned}$$

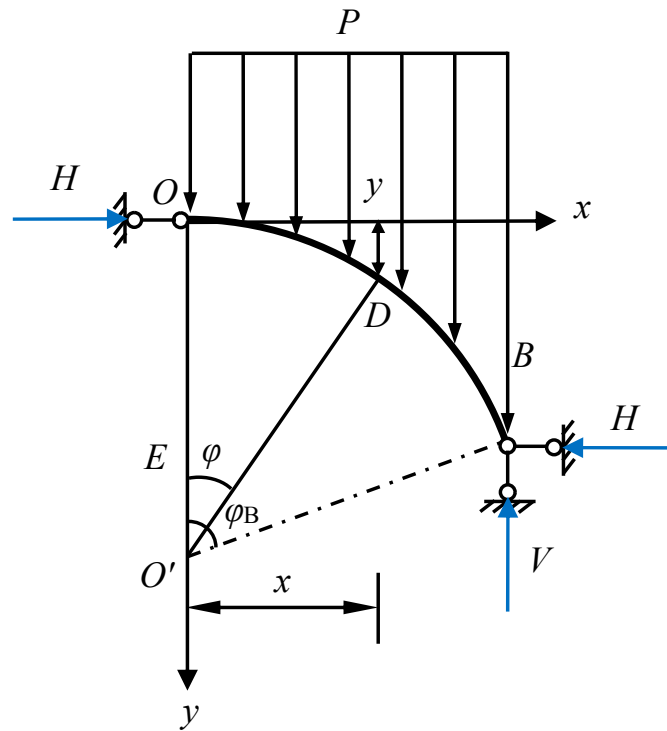


Figure 8. Half-side structure of the three-hinged arch.

The vertical reaction force V of the support is also the total half-span load, which is the same as Formula (29).

2.4.4. Internal Force Calculation Formula of Any Section of the Arch Ring

The force diagram of the isolator of any section of the right half-arch ring of the three-hinged arch is shown in Figure 9. From the force balance, the bending moment, shear force, and axial force formulae of the section at the distance x from point O can be determined as follows:

Bending function equation:

$$\begin{aligned}
 M(\varphi) &= Hy - \frac{P_t}{2} x^2 - \left(x \int_0^x \gamma_2 y dx - \int_0^x \gamma_2 x y dx \right) \\
 &= H(R - R \cos \varphi) - \frac{P_t}{2} R^2 \sin^2 \varphi \\
 &\quad - \gamma_2 R^3 \left(\frac{\sin^2 \varphi}{2} - \frac{\varphi \sin \varphi}{2} - \frac{\sin \varphi \sin 2\varphi}{4} - \frac{\cos^3 \varphi}{3} + \frac{1}{3} \right) \tag{34}
 \end{aligned}$$

Shear force function equation:

$$\begin{aligned}
 Q(\varphi) &= H \sin \varphi - \left(\int_0^x P dx \right) \cos \varphi \\
 &= H \sin \varphi - P_t R \sin \varphi \cos \varphi - \left[\gamma_2 \int_0^\varphi (R - R \cos \varphi) d(R \sin \varphi) \right] \cos \varphi \\
 &= H \sin \varphi - P_t R \sin \varphi \cos \varphi - \gamma_2 R^2 \cos \varphi \left(\sin \varphi - \frac{\varphi}{2} - \frac{\sin 2\varphi}{4} \right) \tag{35}
 \end{aligned}$$

Shear force function equation:

$$\begin{aligned}
 N(\varphi) &= H \cos \varphi - \left(\int_0^x P dx\right) \sin \varphi \\
 &= H \cos \varphi - P_t R \sin^2 \varphi - \left[\gamma_2 \int_0^\varphi (R - R \cos \varphi) d(R \sin \varphi)\right] \sin \varphi \\
 &= H \cos \varphi - P_t R \sin^2 \varphi - \gamma_2 R^2 \sin \varphi \left(\sin \varphi - \frac{\varphi}{2} - \frac{\sin 2\varphi}{4}\right)
 \end{aligned}
 \tag{36}$$

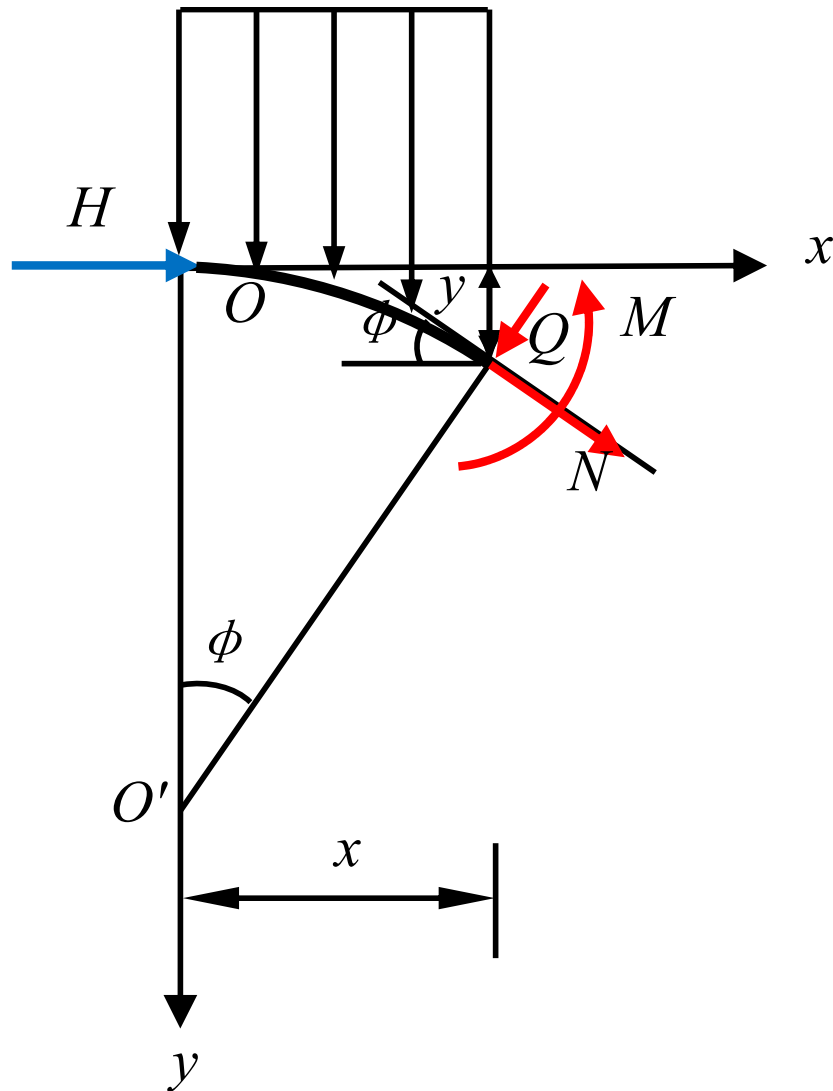


Figure 9. Force diagram of isolated part at any section of the three-hinged arch.

3. Results and Analysis

Based on the obtained size data of a masonry cave dwelling in northern Shaanxi, the selected size parameters of the sample calculation are: cave-dwelling span $l = 3.6$ m, arch ring height $f = 1.5$ m, arch ring thickness $h_1 = 250$ mm, arch ring self-weight $\gamma_1 = 24.8$ kN/m³, the thickness of the covering soil at the vault is $h_2 = 1.0$ m, the self-weight of filling soil is $\gamma_2 = 20$ kN/m³, the uniformly distributed live load on the roof is $q = 2$ kN/m², and the combined value coefficient $\psi = 0.7$. The partial coefficients of the dead load and live load are not considered here, so the load concentration at any cross-section of the arch ring is $P = P_t + 20y = 27.6 + 20y$, the radius of the circular arch is $R = 1.83$ m, and the central angle of the circular half arch is $\varphi_B = 1.3895$ rad.

3.1. Force Calculation Results under the Unhinged Arch Model

From the Formulae (27)–(29), the constraint moment M_B , the horizontal thrust H_B and the vertical force V_B at the arch foot support can be obtained as:

$$M_B = 6.68 \text{ kN}\cdot\text{m}, H_B = 36.27 \text{ kN}, V_B = 63.09 \text{ kN}$$

According to Formulae (30)–(32), the bending moment diagram, shear diagram, and axial diagram of the right half-arch ring within $\varphi \in [0, 1.3895]$ are drawn, as shown in Figure 10. The bending moment diagram and axial force diagram of the left half-arch ring is symmetrical with those of the right half-arch ring under the unhinged arch model, while the shear force diagram is anti-symmetric.

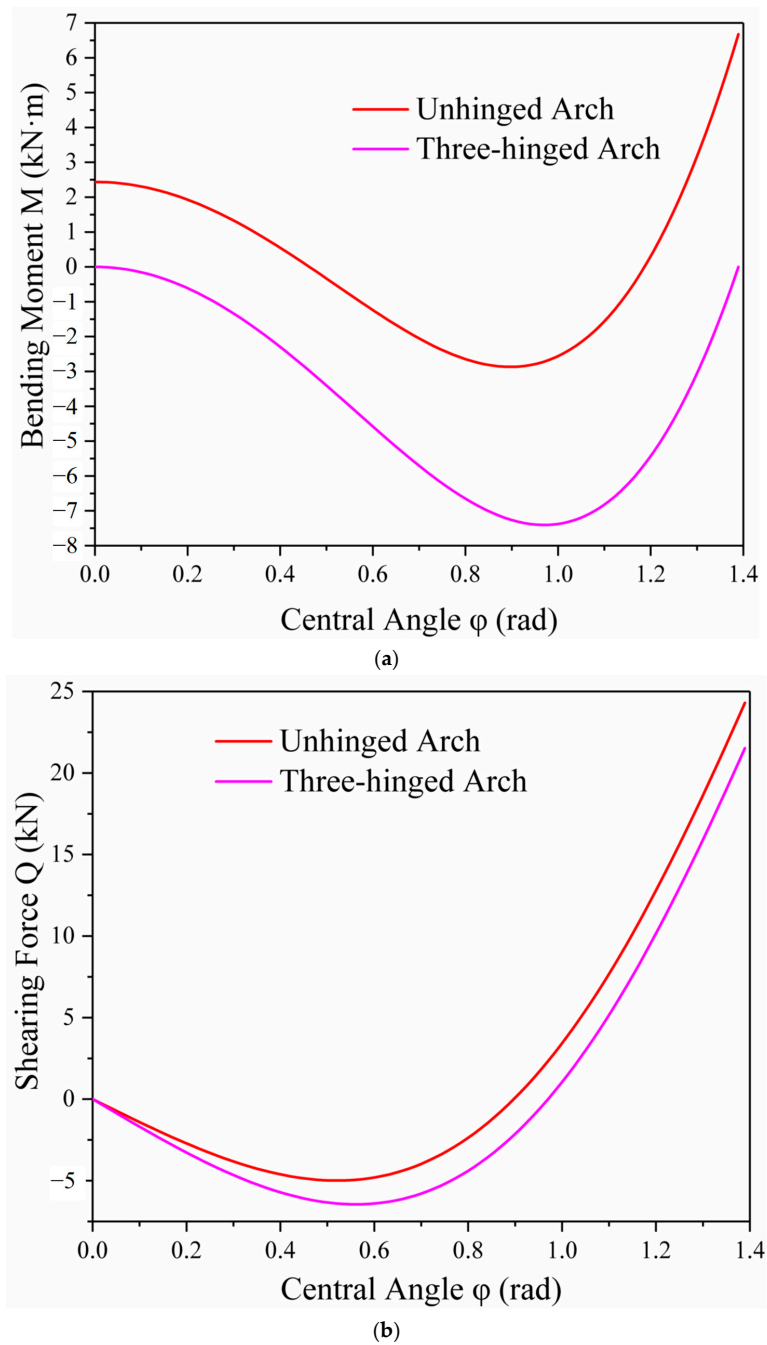


Figure 10. Cont.

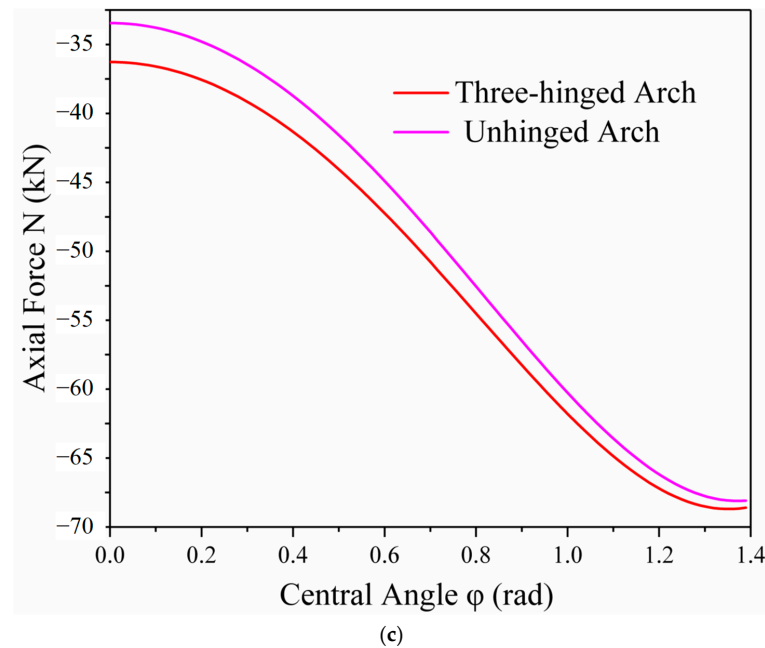


Figure 10. Section internal force of right arch ring according to internal force formula of the unhinged arch and three-hinged arch: (a) bending moment M ; (b) shearing force Q ; and (c) axial force N .

3.2. Force Calculation Results under the Three-Hinged Arch Model

Based on Formulae (29) and (33), the horizontal thrust H and the vertical force V at the arch foot support are:

$$H = 33.45 \text{ kN}, V = 63.09 \text{ kN}$$

According to Formulae (34)–(36), the bending moment diagram, shear force diagram, and axial force diagram of the right half-arch ring in the range of $\varphi \in [0, 1.3895]$ are drawn, as shown in Figure 10. The bending moment diagram and axial force diagram of the left half-arch ring are symmetrical with those of the right half-arch ring under the three-hinged arch model, while the shear force diagram is antisymmetric.

3.3. Comparative Analysis of Calculation Results of the Two Models

Compared with the three-hinged arch, under the same load, the vertical reaction force V of the unhinged arch with the same arch axis is the same, and the horizontal thrust H is extremely close, while the thrust of the unhinged arch is larger, with the difference value of $(36.27 - 33.45)/33.45 = 8\% < 10\%$. The bending moment at the three-hinged arch support is 0, while the restraint moment at the unhinged arch support is 6.68 kN·m.

The internal forces of the unhinged arch and the three-hinged arch at the section of the vault and the arch foot are calculated by Formulae (25)–(29), (35) and (36); they are shown in Table 1. It can be seen that the shear force and axial force of the unhinged arch model are not much different from the three-hinge arch model except for the bending moment in the section of the vault and the arch foot.

Table 1. Internal forces at the section of the vault and the arch foot under the two calculation models.

Calculation Model	Section Position	Bending Moment M (kN·m)	Shearing Force Q (kN)	Axial Force N (kN)
unhinged arch	arch vault	2.44	0	36.27
	arch foot	6.68	24.31	68.59
three-hinged arch	arch vault	0	0	33.45
	arch foot	0	21.52	68.09

It can be seen from Figure 10a that the bending moment of the arch section calculated by the unhinged arch model has two types: internal tension and external tension. There is a reverse bending point on the arch axis, and the maximum external tensile moment reaches 2.87 kN·m, which appears at about one-third of the distance from the arch foot, while the internal maximum tensile moment occurs at the arch foot, reaching 6.68 kN·m. The section bending moment calculated by the three-hinged arch model is only external tension, and the maximum bending moment is 7.41 kN m, which also appears at approximately one-third of the position from the arch foot. However, the absolute value of the maximum bending moment of the section calculated by the two mechanical models is approximately the same, and the difference is only $(7.41 - 6.68)/7.41 = 9\% < 10\%$. According to Figure 10b,c, the shear force and axial force calculated by the two models of the unhinged arch and three-hinged arch are basically the same as the changing trend of the section position; that is, they both gradually increase from the vault to the arch foot. The maximum shear forces of the two models both occur at the support and the values are not much different; the maximum shear force of the section calculated by the unhinged arch model is 24.31 kN, and that of the three-hinged arch model is 21.52 kN, which is slightly smaller than that of the unhinged arch model. The maximum axial forces of the two models occur near the support and the values were close. The maximum axial force of the section calculated by the unhinged arch model was 68.70 kN, and the maximum axial force of the section calculated by the three-hinged arch model was 68.11 kN; the axial force calculated by the unhinged arch was slightly larger. Therefore, it can be concluded that the maximum value of the bending moment, shear force, and axial force calculated by the two mechanical models are relatively close, and the selection of any mechanical model has little influence on the section design and recheck of the arch ring section.

4. Conclusions

A calculation model of the unhinged arch that is closer to the actual force situation is proposed for the arch ring in the masonry cave-dwelling structure. Based on the theory of elastic center in structural mechanics, the unified internal force calculation formula of the arc arch ring in the masonry cave-dwelling structure is deduced by using the principle of force method. Compared with the three-hinged arch calculation model, the force results obtained by the unhinged arch calculation model are not significantly different from the three-hinged arch model. Therefore, it is correct and reliable to use the unhinged arch calculation model for the force of the arch ring in the masonry cave dwelling; both models can be applied to the mechanical analysis of the arch ring. Only the three-hinged arch model is a static structure, which is easy to calculate and widely used, while the unhinged arch model is a super-static structure, which is close to the actual model force but complicated to calculate; the application of the elastic center method makes the calculation much easier and provides a theoretical basis for designers to calculate it more accurately.

In addition to the upper arch ring members, the masonry cave dwelling also has the lower cave-dwelling leg members. Generally, masonry cave dwellings are connected in the form of porous caves. The middle cave-dwelling legs bear the thrust or bending moment transmitted by the arch ring supports on both sides. Because the thrust or bending moment on the left and right sides balance each other and cancel each other out, the middle cave-dwelling legs only bear the vertical reaction force of the support, and the middle cave-dwelling legs are regarded as axial compression members. However, for the side cave-dwelling legs, in addition to bearing the vertical reaction of the support, they must also have the ability to resist the horizontal thrust, which should be regarded as compression-bending members. If the unhinged arch calculation model is adopted, the arch ring support is fixed, and the side cave-dwelling legs have to bear the restraining moment of the support in addition to the horizontal thrust. Compared with the three-hinged arch calculation model, the calculation results obtained by the unhinged arch calculation model are more reliable and safer in the design and calculation of the cave-dwelling leg components. This has a certain theoretical reference value for the construction, reinforcement, and protection

of masonry cave dwellings, and further supplements and improves the design data of cave-dwelling structures.

Author Contributions: Conceptualization, Y.H. and Y.L.; methodology, Y.H.; software, Y.H.; validation, Y.H. and Y.L.; formal analysis, Y.H.; investigation, Y.L.; resources, Y.L.; data curation, Y.H.; writing—original draft preparation, Y.H.; writing—review and editing, Y.H. and Y.L.; visualization, Y.H.; supervision, Y.H.; project administration, Y.H. and Y.L.; funding acquisition, Y.H. All authors have read and agreed to the published version of the manuscript.

Funding: This research was funded by the Natural Science Basic Research Project, the Science & Technology Department of Shaanxi Province, grant number 2022JM-266; National College Students' Innovation and Entrepreneurship Training Program, grant number 202110719057; and the Undergraduate Innovation Project of Yan'an University, grant number D2020134.

Institutional Review Board Statement: Not applicable.

Informed Consent Statement: Not applicable.

Data Availability Statement: The data presented in this study are available upon request from the corresponding author.

Conflicts of Interest: The authors declare no conflict of interest.

References

1. Wang, Z.; Wei, Q.; He, Y. Study on constructive system of green cave dwelling in Loess Plateau—Interpretation with the “regional gene” theory. *J. Zhejiang Univ. Sci. A Int. Appl. Phys. Eng. J.* **2007**, *8*, 1754–1761. [[CrossRef](#)]
2. Abizadeh, E. Investigating effect of using earth-sheltered architecture on energy conservation in cold and mountainous climate; case study: Yakhchal-e Qaem Maqam, Basement of Sharbat Oqli House, and Cistern of Parvin Etesami House. *Iran Energy Assoc.* **1986**, *3*, 167–169.
3. Staniec, M.; Nowak, H. Analysis of the earth-sheltered buildings' heating and cooling energy demand depending on type of soil. *Arch. Civ. Mech. Eng.* **2011**, *11*, 221–235. [[CrossRef](#)]
4. Hayashi, Y. The future of earth-sheltered architecture in China's farming villages. *Tunn. Undergr. Space Technol.* **1986**, *1*, 167–169. [[CrossRef](#)]
5. Ruston, S.A. Earth Sheltered Architecture: An Environmentally Appropriate Response. Master's Thesis, University of California, OKBerkeley, CA, USA, 1985.
6. Golany, G.S. *Earth-Sheltered Habitat: History, Architecture, and Urban Design*; Van Nostrand Reinhold Co.: New York, NY, USA, 1983.
7. Tong, L.P.; Han, C.P. Earth-arched structural systems of primitive earth-sheltered dwelling. *Constr. Technol.* **2008**, *6*, 113–115, 118.
8. Tong, L.P.; Han, C.P. Study on the structural properties of self-support systems for earth-sheltered dwelling. *Sichuan Build. Sci.* **2009**, *35*, 71–73.
9. Hao, Y.; Liang, X.; Lan, Y. Research on the static behavior and strengthening methods of single-hole loess cave dwelling by cliff in Yan'an of northern shaanxi. *Henan Sci.* **2016**, *34*, 1852–1857.
10. Chen, R.F. Scientific Research on the Traditional Construction of Dikeng Cave Dwellings. Master's Thesis, Zhengzhou University, Zhengzhou, China, 2011.
11. Hao, Y.; Liang, X.; Lan, Y. Numerical Simulation and Dynamic Analysis of Single-hole Cliff-side Loess Cave Dwelling under Seismic Actions. *Gefluids* **2021**, *2021*, 6890445. [[CrossRef](#)]
12. Yang, K.; Zhang, F.L.; Zhu, W.W.; Xue, J.Y.; Zhou, H.L.; Dai, M.X. Stability analysis of loess cave dwelling by cliff based on strength reduction method. *Ind. Constr.* **2019**, *49*, 25–30.
13. Wang, N.Q.; Zhang, S. Analysis of stability of cave dwellings based on orthogonal design. *Sci. Technol. Eng.* **2017**, *17*, 119–124.
14. Wu, W.L.; Yang, H.X. Stability analysis of the loess cave dwelling in Shanbei region using comsol. *Ind. Constr.* **2017**, *47*, 119–122.
15. Guo, P.G. Stability analysis of loess cave dwellings under longitudinal earthquake. *Earthq. Resist. Eng. Retrofit.* **2016**, *38*, 133–138.
16. Guo, P.G.; Tong, L.P. Influence of crosswise earthquake on loess cave dwellings' stability. *Earthq. Eng. Eng. Dyn.* **2015**, *35*, 56–63.
17. Wu, W.; Ji, D. Using FLAC3D to simulation and analysis of cave dwelling stability. *Int. J. Digit. Content Technol. Its Appl.* **2012**. [[CrossRef](#)]
18. Wang, N.Q.; Zhang, S. Quantitative evaluation of stability on loess cave dwellings based on blind data theory. *Chin. J. Undergr. Space Eng.* **2017**, *13*, 822–827.
19. Wu, C.J.; Gan, Z.M.; Meng, C.P. Stability of cave dwelling of loess hills in north part of Shaanxi province. *J. Shaanxi Norm. Univ. Nat. Sci. Ed.* **2005**, *3*, 119–122.
20. Han, J.M.; Su, S.Q. Stability analysis of weibeii pitted loess cave dwellings in rainfall infiltration. *J. Archit. Civ. Eng.* **2012**, *29*, 104–110.
21. Bai, B.; Nie, Q.; Zhang, Y.; Wang, X.; Hu, W. Cotransport of heavy metals and SiO₂ particles at different temperatures by seepage. *J. Hydrol.* **2021**, *597*, 125771. [[CrossRef](#)]

22. Xue, J.Y.; Zhao, X.B.; Zhang, F.L. Shaking table test on model structure of underground loess cave. *J. Build. Struct.* **2021**, *42*, 14–23.
23. Liu, B.T.; Liu, X.L.; Zhang, S. Analysis of pressure arch effect and failure mode of cliff-type cave dwellings with different covering soil thickness. *China Non-Met. Miner. Ind.* **2018**, *38*, 36–40, 44.
24. Zhang, F.L.; Tian, P.G.; Zhu, W.W.; Yang, K.; Hu, X.F.; Fan, D.G. *Analysis of Mechanical Properties of Cave Dwelling Structure and Research on Reinforcement and Protection Technology*; China Construction Industry Press: Beijing, China, 2020.
25. Yuan, B.; Li, Z.; Chen, Y.; Ni, H.; Zhao, Z.; Chen, W.; Zhao, J. Mechanical and microstructural properties of recycling granite residual soil reinforced with glass fiber and liquid-modified polyvinyl alcohol polymer. *Chemosphere* **2021**, *268*, 131652. [[CrossRef](#)]
26. Guan, D.; Yang, N.; Lai, J.; Siu MF, F.; Jing, X.; Lau, C.K. Kinematic modeling and constraint analysis for robotic excavator operations in piling construction. *Autom. Constr.* **2021**, *126*, 103666. [[CrossRef](#)]
27. Wang, F.J.; Liu, R.S.; Ma, Z.H. Damage measures analysis of independent cave dwelling under earthquake. *Sci. Technol. Eng.* **2018**, *18*, 281–286.
28. Yan, Y.M. Force analysis and section calculation of arch ring of stone-built cave. *Proc. Fifth Natl. Conf. Struct. Eng.* **1996**, *1*, 672–675.
29. Yan, Y.M.; Guo, B.S. Research on the reasonable arch ring of stone-built cave. *Proc. Fourth Natl. Conf. Struct. Eng. Part 2* **1995**, *3*, 655–658.
30. Zhang, Y.X.; Tian, X.Y. Destroy causes of cave dwelling and its cure measure. *J. Northwest Univ. Agric. For. Sci. Technol. Nat. Sci. Ed.* **2004**, *32*, 145–149.
31. Huang, C.H.; Wang, Z.J. Structure analysis on the cave dwelling. *J. Chang. Inst. Technol. Nat. Sci. Ed.* **2009**, *10*, 46–48.
32. Structural Mechanics Teaching Team of Chongqing University. *Structural Mechanics*; Higher Education Press: Beijing, China, 2020.
33. Bao, S.H. *Structural Mechanics*; Wuhan University of Technology Press: Wuhan, China, 2008.

Disclaimer/Publisher’s Note: The statements, opinions and data contained in all publications are solely those of the individual author(s) and contributor(s) and not of MDPI and/or the editor(s). MDPI and/or the editor(s) disclaim responsibility for any injury to people or property resulting from any ideas, methods, instructions or products referred to in the content.